The Astrophysical Journal, 546:234–247, 2001 January 1

A NEW MODEL FOR THE SPIRAL STRUCTURE OF THE GALAXY: SUPERPOSITION OF 2- AND 4-ARMED PATTERNS

J. R. D. Lépine
Instituto Astronômico e Geofisico da Universidade de Sao Paulo, Av. Miguel Stefano 4200, 04301-904 São Paulo, SP, Brazil; jacques@iagusp.usp.br
and
Yu. N. Mishurov and S. Yu. Dedikov
Space Research Department, Rostov State University, 5 Zorge, Rostov-on-Don, 344090, Russia; mishurov@phys.rnd.runnet.ru
Received 1999 December 2; accepted 2000 July 26

ABSTRACT

We investigate the possibility of describing the spiral pattern of the Milky Way in terms of a model of superposition of 2- and 4-armed wave harmonics (the simplest description, besides pure modes). Two complementary methods are used: a study of stellar kinematics and direct tracing of positions of spiral arms. In the first method, the parameters of the Galactic rotation curve and the free parameters of the spiral density waves were obtained from Cepheid kinematics, under different assumptions. To make visible the structure corresponding to these models, we computed the evolution of an ensemble of N particles, simulating the ISM clouds, in the perturbed Galactic gravitational field. In the second method, we present a new analysis of the longitude-velocity (l-v) diagram of the sample of Galactic H II regions, converting positions of spiral arms in the Galactic plane into loci of these arms in the l-v diagram. Both methods indicate that the "self-sustained" model, in which the 2-armed and 4-armed mode have different pitch angles (6° and 12°, respectively), is a good description of the disk structure. An important conclusion is that the Sun happens to be practically at the corotation circle. As an additional result of our study we propose an independent test for localization of the corotation circle in a spiral galaxy: a gap in the radial distribution of interstellar gas has to be observed in the corotation region.

Subject headings: Galaxy: kinematics and dynamics — Galaxy: structure

1. INTRODUCTION

A good understanding of the large-scale spiral structure of the Galaxy has not been reached up to the present. Georgelin & Georgelin (1976, hereafter GG) derived a 4-armed pattern, based on an analysis of the distribution of giant H II regions. According to Vallée (1995) most research supports the 4-armed pattern, although there are discordant opinions; for instance, Bash (1981), on the basis of the same data that were used by GG, finds the pattern to be 2-armed, similar to the first spiral structure model proposed by Lin, Yuan, & Shu (1969, hereafter LYS). But even if we accept that there is observational evidence in favor of a 4-armed structure, the theory of an extended 4-armed pattern is not well established, and observational difficulties remain.

One problem was noted by Amaral & Lépine (1997, hereafter AL). They pointed out that as is well known, the spiral waves exist between the inner and the outer Lindblad resonances. For the pure 4-armed pattern this region happens to be much shorter than the range of the observed spiral pattern. AL then proposed a representation of the Galactic spiral structure as a superposition of 2- and 4-armed (2+4-armed) wave patterns, to account for the number of arms and for the existence of arms over a wider range of radii. In AL's model, two arms of the 4-armed component are coincident with the 2-armed component, so that the Galaxy looks 4-armed. However, there are theoretical arguments discussed in the present paper suggesting that 2- and 4-armed patterns should have different pitch angles, so that the solution proposed by AL is not very satisfactory.

Furthermore, a representation of the Galactic pattern by a pure 4-armed pattern (or by a model like that of AL; see also Englmaier & Gerhard 1999, hereafter EG) is a very ideal one. For instance, external galaxies often demonstrate much more complicated structures with branching of arms and bridges between them, e.g., the galaxy M101. These facts suggest that such patterns could be represented by a superposition of different wave harmonics with different pitch angles. An attractive aspect of such a model with arms of different pitch angles is that it naturally accounts for bifurcation of arms. A detailed Fourier analysis of external galaxies in terms of spiral modes, performed by Puerari & Dottori (1992), indicates that in the cases in which the 2-armed and 4-armed patterns are prominent, they indeed have different pitch angles.

The structure of the Milky Way is perhaps similarly complicated. In fact, there are observed arms in the Galaxy that do not fit in a simple 4-armed structure. For instance, outside the solar circle, around longitudes 210°–260°, three arms are clearly visible, in H I and in *IRAS* sources (Kerr 1969; Wouterloot et al. 1990), but they are not expected from a 4-armed model that fits the tangential directions of the inner parts of the Galaxy (e.g., Ortiz & Lépine 1993).

The main goal of this paper is to investigate if a superposition of 2+4-armed wave harmonics is a good representation of the spiral structure of the Galaxy. Two different approaches are used. In one approach, we analyze the Cepheid kinematics, using a model that takes into consideration the perturbation of the stellar velocity field by the spiral arms, to derive the structural parameters of the gravitational field in the Galactic disk. And, since the structure of the perturbation potential does not necessarily correspond to the visible structure, we performed a many-particle simulation of gasdynamics in this potential, to outline the predicted visible structure. In the second approach, we directly analyze the visible structure by means of the sample of H II regions, since these objects are recognized as the best large-scale tracers of the galactic structure. We present a new analysis of the observed longitude-velocity (l-v) diagram of an up-to-date sample of H II regions, deriving from it the position of the spiral arms, and we compare the observed *l-v* diagram with those computed from our gasdynamics simulations.

The Cepheid kinematics analysis is performed for two different models of 2+4-armed structures, and the results are compared with previous calculations of pure 2-armed and pure 4-armed (Mishurov & Zenina 1999, hereafter MZ). An important result is that for the more realistic model, the Sun lies very close to the corotation region. Furthermore, our simulation revealed the interesting effect of gas pumping out from the corotation. This suggests that in spiral galaxies, there must be a gas deficiency in a region near the corotation circle. This phenomenon explains the lack of atomic hydrogen in a ringlike region near the solar circle derived by Kerr (1969) and by Burton (1976), which have remained not understood up to now. We propose this effect as an independent test for localization of a corotation circle in external spiral galaxies.

2. METHOD OF ESTIMATION OF THE STRUCTURAL PARAMETERS

2.1. *Description of the Model*

The derivation of the spiral wave parameters is based on the statistical analysis of stellar motion in the Galaxy (see, e.g., Crezé & Mennessier 1973, hereafter CM; MZ; Mishurov et al. 1997). We look for the parameters describing the structure of the galactic gravitational field. This structure is not directly visible. However, the gravitational field determines the stellar motion, and in particular, the spiral perturbation of the field causes the stellar motion to deviate from rotation symmetry. Hence, analyzing the stellar velocity field in the framework of some model, we can derive the parameters of the density waves and those of the galactic rotation. We next briefly describe the method.

In the presence of the galactic spiral density waves the gravitational potential of the Galaxy φ_G may be represented as the sum

$$\varphi_G = \varphi_0 + \varphi_S , \tag{1}$$

where φ_0 is the unperturbed regular axissymmetric part of the potential that determines the Galaxy equilibrium as a whole and φ_S is the perturbation due to spiral density waves.

In accordance with equation (1) we divide the systematic velocity of any star into two parts: the unperturbed velocity with components $\{0, \Omega R\}$ and a perturbation $\{\tilde{v}_R, \tilde{v}_\vartheta\}$. Here we adopt the cylindrical coordinate system R, ϑ, z with the origin at the Galactic center, the z-axis being directed along the axis of the Galactic rotation. The quantities in the braces are the radial and the azimuthal components of the corresponding velocities in the Galactic plane, and Ω is the angular rotation velocity of the Galactic disk. The equilibrium corresponds to $\varphi'_0 = \Omega^2 R$ (hereafter the prime denotes a derivative with respect to R).

Following CM, the components of the stellar velocities relative to the Sun in the direction of the line of sight (v_r) and in the transversal direction (v_l), oriented along increasing Galactic longitude, can be written as

$$\begin{aligned} v_r = \{&[-2A + 0.5\, R_\odot \Omega''_\odot(R-R_\odot)](R-R_\odot)\sin l \\ &+\tilde{v}_\vartheta \sin(l+\vartheta) - \tilde{v}_R \cos(l+\vartheta) \\ &+u_\odot \cos l - v_\odot \sin l\}\cos b - w_\odot \sin b , \end{aligned} \tag{2}$$

$$\begin{aligned} v_l = &-\Omega_\odot r \cos b + [-2A + 0.5\, R_\odot \Omega''_\odot(R-R_\odot)] \\ &\times(R-R_\odot)\cos l + \tilde{v}_\vartheta \cos(l+\vartheta) \\ &+\tilde{v}_R \sin(l+\vartheta) - u_\odot \sin l - v_\odot \cos l , \end{aligned} \tag{3}$$

where $\Omega_\odot$ is the rotational velocity of the Galaxy at the distance of the Sun (hereafter the subscript "Sun symbol" denotes values corresponding to the position of the Sun), $A = -0.5\, R_\odot \Omega'_\odot$ is Oort's A-constant, l and b are the Galactic longitude and latitude of the star, r is its distance from the Sun, and $u_\odot$, $v_\odot$, and $w_\odot$ are the components of the solar peculiar velocities.

Now let us represent the perturbed potential in the form of superposition of two harmonics:

$$\varphi_S = \varphi_{S2} + \varphi_{S4} , \tag{4}$$

where

$$\varphi_{Sm} = A_m \cos \chi_m , \tag{5}$$

here A_m is the amplitude of the mth harmonic; χ_m is the corresponding wave phase:

$$\chi_m = m[(\cot i_m)\ln(R/R_\odot) - \vartheta] + \chi_{\odot m} , \tag{6}$$

where m is the azimuthal wavenumber, i.e., the number of arms for a given harmonic, i_m is the corresponding pitch angle of an arm; and $\chi_{\odot m}$ is the initial phase or the wave phase at the Sun position. From equation (6) it is seen that this last parameter fixes the mth harmonic position relative to the Sun.

Following the density wave theory we can write

$$\tilde{v}_R = f_{R2} \cos \chi_2 + f_{R4} \cos \chi_4 , \tag{7}$$

$$\tilde{v}_\vartheta = f_{\vartheta 2} \sin \chi_2 + f_{\vartheta 4} \sin \chi_4 , \tag{8}$$

where f_{Rm} and $f_{\vartheta m}$ are the amplitudes of the mth harmonic.

For tightly-wound spirals ($|i_m| \ll 1$—the usual WKB approximation in LYS theory) the quantities f_{Rm}, $f_{\vartheta m}$, and i_m are slowly varying functions in R compared to the wave phase χ_m. Thus as a first step we can consider them to be constant. Hence, using a statistical method we can derive by means of equations (2), (3), (6), (7), and (8) the parameters of the rotation curve $\Omega_\odot$, A, $R_\odot \Omega''_\odot$, the components of the solar peculiar velocity $u_\odot$, $v_\odot$ ($w_\odot$ cannot be derived using distant stars, and we adopt $w_\odot = 7$ km s^{-1}; see also Pont, Mayor, & Burki 1994), and the parameters of the spiral waves f_{Rm}, $f_{\vartheta m}$, i_m, $\chi_{\odot m}$. The statistical method consists in comparing calculated and observed stellar velocities, over a sample of stars with well-known distances, and obtaining the best set of parameters.

At the next stage we use the density wave theory to compute the angular rotation velocity of the pattern Ω_{pm}, the corresponding corotation radius R_{cm} and the amplitude of disturbed spiral gravitational field A_m. These calculations are done in the following manner.

According to LYS:

$$f_{Rm} = A_m \frac{k_m}{\kappa}\left(\frac{\nu_m}{1-\nu_m^2}\right) F^{(1)}_{\nu_m}(x_m) \tag{9}$$

$$f_{\vartheta m} = -A_m \frac{k_m}{2\Omega}\left(\frac{1}{1-\nu_m^2}\right) F^{(2)}_{\nu_m}(x_m) \tag{10}$$

where

$$k_m = m \cot i_m / R \tag{11}$$

is the radial wavenumber, $\kappa = 2\Omega(1 - A/\Omega)^{1/2}$ is the epicyclical frequency,

$$\nu_m = \frac{m(\Omega_{pm} - \Omega)}{\kappa} \qquad (12)$$

is the dimensionless spiral wave frequency,

$$x_m = \left(\frac{k_m c_R}{\kappa}\right)^2 , \qquad (13)$$

c_R^2 is the dispersion of radial stellar velocities, and $F_\nu^{(1)}(x)$ and $F_\nu^{(2)}(x)$ are the reduction factors

$$F_\nu^{(1)}(x) = \frac{1 - \nu^2}{x}\left[1 - \frac{\nu\pi}{\sin(\nu\pi)}\frac{1}{2\pi} \times \int_{-\pi}^{\pi} e^{-x(1+\cos s)}\cos(\nu s)ds\right], \qquad (14)$$

$$F_\nu^{(2)}(x) = -\frac{(1-\nu^2)(\nu\pi)}{\sin(\nu\pi)}\frac{\partial}{\partial x}\left[\frac{1}{2\pi}\int_{-\pi}^{\pi} e^{-x(1+\cos s)}\cos(\nu s)ds\right]. \qquad (15)$$

Equations (9)–(15) and the quantities f_{Rm}, $f_{\vartheta m}$, and i_m, as well the parameters of the rotation curve, derived in the statistical part of the problem, enable us to compute the amplitude of spiral gravitational field A_m and the difference $\Delta\Omega_{pm} = \Omega_{pm} - \Omega_\odot$. By equating $\Omega(R_{cm}) = \Omega_{pm}$ we find the corotation radius and the displacement $\Delta R_m = R_{cm} - R_\odot$ of the Sun relative to the corotation radius.

Notice here some features of our model. In the first approach adopted in this paper, the structure of our Galaxy is generated by a bar in the Galactic center. The bar is considered as the source of the spiral waves that propagate outward from the inner Lindblad resonance; this does not mean that the potential of the bar extends to large radii. As discussed by Lépine & Leroy (2000), there is a large class of galaxies in which the arms are clearly tied to the bar, and there is observational evidence that our Galaxy is of this type. In the LYS theory the spiral waves are self-sustained and the disturbances of the gravitational field are mainly due to the density waves which propagate in the Galactic stellar disk. For the stationary structure, the angular rotation velocity of the pattern is determined by the bar rotation. Hence, the value Ω_{pm} does not depend on m and the corotation radius does not depend on m either. The corresponding dispersion relation imposes a connection between i_2 and i_4. Indeed, the solution of the dispersion relation for spiral waves relative to the radial wavenumber k_m in the vicinity of corotation does not depend on m (Shu 1970; Mark 1976). Since $\cot i_m = k_m R/m$, we have

$$\cot i_2 = 2 \cot i_4 . \qquad (16)$$

Therefore, in this approach, the 2-armed pattern is tighter wound (about twice for small-pitch angles) than the 4-armed one.

The above argument is strictly held in the vicinity of the corotation circle (notice here that according to Marochnik et al. 1997, CM, MZ, AL, etc., the Sun is situated just near the corotation). However, since the radial wavenumber and consequently the pitch angle are slowly varying functions of R (LYS), relation (16) can be used for a sufficiently wide region around the corotation radius, except for the vicinity of Lindblad resonances.

In the second approach considered in the present paper the perturbations of the gravitational potential are represented by a superposition of 2+4-armed harmonics, but in contrast to the previous case the 4-armed pattern has the same pitch angle as the 2-armed, and 2 of the 4-armed components coincide with the 2-armed pattern (e.g., EG; AL):

$$\chi_4 = 2\chi_2 \ ; \quad i_4 = i_2 . \qquad (17)$$

In what follows we shall analyze both approaches. We call them the self-sustained model (approach 1) and the bar-dominated model (approach 2).

An important peculiarity of our task is that some of the wave parameters, $f_{R2}, f_{\vartheta 2}, f_{R4}, f_{\vartheta 4}$, i_2 (i_4 is fixed automatically in both approaches), $\chi_{\odot 2}$, and $\chi_{\odot 4}$, obey nonlinear statistics. In the self-sustained model $\chi_{\odot 2}$ and $\chi_{\odot 4}$ are considered to be independent quantities; in the bar-dominated approach, these values are connected by equation (17). In order to avoid nonlinearity, CM expanded equations (6)–(8) in a series over a parameter $rm \cot i_m/R_\odot$ and restricted themselves to first-order members. This expansion enables us to reduce the task to a linear one, but the procedure leads to a very strong limitation on stellar distances in a sample: $r \ll R_\odot/(m \cot i_m)$ (for $m = 4$, $i_m \sim 12°$, and $R_\odot \sim 8$ kpc, this condition becomes $r \ll 0.4$ kpc).

In our sample the stars are spread over a much wider distance from the Sun (up to a distance $r \sim 4$ kpc)—a very important point for the derivation of reliable structural parameters (see below). That is why we do not use the CM method and treat the mentioned parameters using nonlinear statistics. The method of solving the statistical part of the problem in this case is as follows (see details in MZ and Mishurov et al. 1997).

First, note that if we fix i_2, $\chi_{\odot 2}$, and $\chi_{\odot 4}$ (in the bar-dominated model it is sufficient to fix only i_2 and $\chi_{\odot 2}$; see eq. [17]), the task reduces to a linear problem over the other parameters. So the strategy to localize the global minimum for the residual (δ^2) is as follows. Let us adopt some values for the above quantities and look for the minimum of residual over the other parameters by means of the least-squares method (we denote this minimum by $\Delta = \min_{i_2,\chi_{\odot 2},\chi_{\odot 4}}(\delta^2)$). Then we change values of i_2, $\chi_{\odot 2}$, and $\chi_{\odot 4}$, and again derive Δ, and so on. After that, we construct the net Δ as a function of i_2, $\chi_{\odot 2}$, and $\chi_{\odot 4}$. Of course, we cannot imagine this function visually, but we can construct the surface, say, $\Delta(\chi_{\odot 2}, \chi_{\odot 4})$ for a set of values i_2 and check by eye localization of the global minimum of the residual. After the minimum is localized, we define more exactly the parameters and the covariation matrix of errors by means of a linearization procedure (Draper & Smith 1981).

We now briefly comment on our choice of $R_\odot$, which is not an adjusted parameter. The determinations of this quantity in the literature span a relatively wide range. For instance, Feast & Whitelock (1997) give 8.5 kpc, the value recommended by IAU, whereas the only direct measurement (Reid 1993) gives 7.2 kpc. Ollin & Merrefield (1998) find that a consistent picture is only obtained with 7.1 kpc. However, as was shown by MZ, the results of determining the parameters of the galactic structure change only slightly with variation of $R_\odot$. Bearing this in mind, and in order to compare the present results with the previous ones of MZ, the value $R_\odot = 7.5$ kpc was adopted.

2.2. *The Sample of Cepheids*

Before discussing the stellar sample used in our work, let us comment on some reasons for our choice. Radio or infrared data are often used in studies of the large-scale structure of the Galaxy. These have some value, since the sources can be seen at very large distances, up to the opposite end of the Galaxy. However, they have a defect as well, which is the fact that the distance to a selected region is not obtained independently but is derived from the rotation curve, with few exceptions. In this process, effects that were not included in the model of medium motion in the Galaxy, like perturbations due to spiral arms, etc., can appreciably affect the resulting picture. On the other hand, the stellar data give both velocities and distances derived independently, but as a rule stars can only be seen in a smaller neighborhood of the Sun. This is an important point to be considered, since a star sample (even sufficiently large in number) can only be taken as representative for our task if it occupies a space volume in the Galaxy comparable to the typical scale length of the structures under consideration.

The classical Cepheids are the most convenient objects for solving the problem that we formulated. They are bright stars seen at large distances from the Sun, comparable with the interarm space. The distances for Cepheids can be obtained from the period-luminosity relation. In our work the distances are based on the results of photoelectric photometry by Berdnikov (1987); they are the most accurate and homogeneous distance scale.

As observational material, we used the line-of-sight velocities from Pont et al. (1994), Gorynya et al. (1996), and Caldwell & Coulson (1987) the proper motions from *Hipparcos* catalog (ESA 1997), the photometric data of Berdnikov (1987), and the distances according to Berdnikov et al. (1996; see also Dambis 1995). From these data were excluded the stars with $|z| > 0.5$ kpc (Lewis 1990; Pont et al. 1994) and those whose proper motions are more than 200 km s^{-1}. In all samples, there are 237 values for v_r and 130 for v_l. The stars mainly appear to be situated within $r \leq 4$ kpc, so they occupy a domain of the order of 8 kpc in diameter. The sample is the same used by MZ, who investigated pure spiral modes ($m = 2$ and $m = 4$), so that the results of the two works can be easily compared.[1]

3. RESULTS OF CEPHEID KINEMATICS ANALYSIS

Let us discuss separately the results derived for the two models studied in this work. Note that both models are a superposition of 2-armed and 4-armed patterns. In our first model the 4-armed pattern has a pitch angle about twice that of the 2-armed one, while in the other model the two components have the same pitch angle. These are the simplest models one can think of, besides the pure 2-armed or pure 4-armed models, already discussed by MZ.

3.1. *The Self-sustained Model*

The surfaces $\Delta(\chi_{\odot 2}, \chi_{\odot 4})$ constructed over the Cepheid sample, were calculated for i_2 in the range $-4°$ to $-10°$. They are given for three values of i_2 in Figure 1, for illustration. One can easily see the global minimum in the vicinity of $i_2 \approx -6°$. The final values of the parameters with their errors are given in Table 1.

First of all, we notice the significant decrease of the residual min(δ^2) in this case, in comparison with the ones for single harmonic $m = 2$ or $m = 4$ studied by MZ (see their Table 1, runs 3 and 8). As was shown in that work, the inclusion of the spiral perturbation in stellar motion happens to be significant. However, MZ could not make a choice between the two alternatives that they investigated.

Now, by means of an F-test, we can show that the hypothesis adopted by MZ, that the pattern can be described with one harmonic ($m = 2$ or $m = 4$), must be rejected in favor of the hypothesis tested in the present work, that the pattern is well represented by superposition of 2+4-armed pattern. In other words, the representation of the galactic structure by a superposition of 2+4-harmonics is clearly preferable to the one that uses a single harmonic.

In our model, the quantities $\Delta\Omega_m$ and ΔR_m can both be calculated from the parameters obtained for the components $m = 2$ and $m = 4$. It has not been hitherto obvious that for different m the quantities happen to be the same as we have supposed above. But our calculations lead to very close values for the corresponding quantities: $\Delta\Omega_2 = 0.15$ km s^{-1} kpc^{-1} and $\Delta\Omega_4 = 0.18$ km s^{-1} kpc^{-1}; accordingly, $\Delta R_2 = -0.03$ kpc and $\Delta R_4 = -0.04$ kpc, the standard (i.e., 68%) confidence intervals being for $\Delta\Omega_2$: -0.61 to 1.02 km s^{-1} kpc^{-1}; for $\Delta\Omega_4$: 0.13 to 0.24 km s^{-1}kpc^{-1}; for ΔR_2: -0.21 to 0.13 kpc; for ΔR_4: -0.05 to 0.03 kpc. The confidence intervals were estimated by means of numerical experiments making use of random number generation of parameters, giving the resulting distribution of ΔR_m or $\Delta\Omega_m$. The method is described in detail by MZ. Hence, in the model under consideration the Sun is practically situated at the corotation circle, slightly beyond it.

We could not estimate with reasonable accuracy the values of the amplitudes of the spiral gravitational field A_2 and A_4 (this is expected from linear perturbation theory). However, their ratio is derived very precisely: $A_2/A_4 = 0.79$, the standard confidence interval being 0.77–0.80.

The locus of minima for φ_{Sm} are shown in Figure 2; they are the lines of constant phase χ_m on the Galactic plane corresponding to min (φ_{Sm}). From this figure the pattern may be thought to be a 6-armed one. However, this is not the case in our model, in which the potential perturbation is represented by cosine functions. Indeed, simple computation shows that for the above derived parameters the sum $\varphi_{S2} + \varphi_{S4}$ has at most four minima over ϑ for a fixed R. It would only be possible to obtain six minima (in the frame of a 2+4 armed model) if the potential were represented by some function presenting sharp minima, in contrast to the cosine function. The visible structure derived by means of particle-cloud simulations and given in § 4 supports this point of view. Of course, the actual structure of the Galaxy may happen to be more complicated, e.g., due to higher wave harmonics or to special effects at the corotation (Mark 1976). However, these possibilities are beyond the present investigation.

3.2. *The Bar-dominated Model*

Let us clarify the meaning of the term "bar-dominated," in the present context. We only mean that the strong effect of a bar could be a way to explain similar pitch angles for the 2-armed and 4-armed components. We do not pretend that this is the only way to deal with the presence of a bar, or that a bar necessarily produces the kind of pattern that we are studying.

In this case the results are quite different from the previous ones. The pattern rotation velocities are, for $m = 2$,

[1] The corresponding data are available in electronic form at: http://www.phys.rsu.ru/~cosmos.

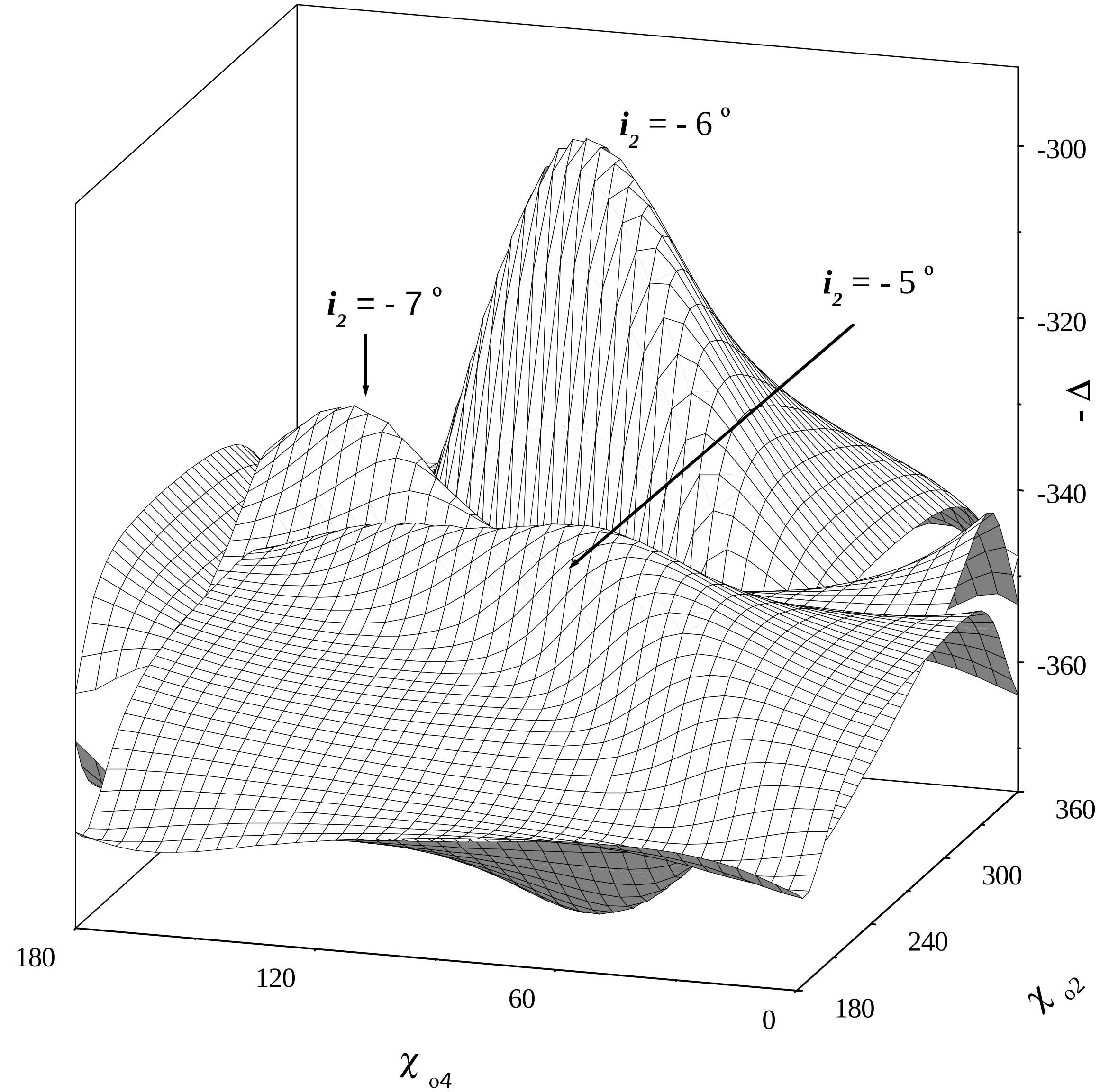

FIG. 1.—Surfaces of Δ as a function of $\chi_{\odot 2}$ and $\chi_{\odot 4}$ for three values of pitch angle i_2. For a given set of parameters $\chi_{\odot 2}$, $\chi_{\odot 4}$, and i_2, Δ is the minimum value of the residual obtained by fitting the remaining parameters of the model to the data. For better visual perception, $-\Delta$ is presented, so that the mimima appear like maxima.

$\Omega_{p2} = 35.0$ km s^{-1} kpc^{-1}, and for $m = 4$, $\Omega_{p4} = 29.2$ km s^{-1} kpc^{-1}. So the main requirement of the model, that the pattern rotation velocity and the corotation radius should not depend on *m*, is not held. Indeed, for the parameters of the rotation curve of Table 1 and the above value for Ω_{p2}, the corotation radius R_{c2} does not exist as a real number at all (this is mainly because the second derivative $R_\odot \Omega''_\odot$ is negative). On the other hand, for $m = 4$, $R_{c4} = 5.4$ kpc. Further, in this case the ratio $A_2/A_4 \approx 8.21$ is very large. So the visible pattern happens to be almost purely 2-armed.

At last, the residual $\delta^2 \approx 220$ is significantly greater than in the previous approach and happens to be very close to the values for pure $m = 2$ and pure $m = 4$ solutions (see Table 1 of MZ, runs 3 and 8). Hence, it is impossible to make a choice between pure $m = 2$, pure $m = 4$, or a superposition of $2+4$-modes in the bar-dominated approach.

This result seems to be very important. Indeed, one usually expects that the structure could be better represented by a superposition of several harmonics than by a single harmonic. However, this is true only if the nature of harmonics is chosen correctly. The above result shows that the spiral pattern cannot be satisfactorily represented in the frame work of the discussed model.

The above statistical analysis of the large-scale stellar kinematics of Cepheid stars leads us to the conclusion that the preferable solution for the spiral structure of the Galaxy is a superposition of self-sustained $2+4$-harmonics of density waves, and that the Sun is situated very close to the corotation circle.

4. PREDICTED VISIBLE LARGE-SCALE STRUCTURE OF THE GALAXY

The above-derived structure of the gravitational field and of the stellar velocity field in the Galaxy is not directly seen. To make it visible, the evolution of a gas-cloud ensemble in the galactic gravitational field perturbed by spiral arms will be considered next. Following Roberts & Hausman (1984, hereafter RH), we simulate the interstellar clouds by ballis-

TABLE 1

MODEL PARAMETERS AND THEIR ERRORS DERIVED BY MEANS OF STATISTICAL ANALYSIS

Approach	$\Omega_\odot$ (km s^{-1} kpc^{-1})	A (km s^{-1} kpc^{-1})	$R_\odot \Omega''_\odot$ (km s^{-1} kpc^{-2})	$u_\odot$ (km s^{-1})	$v_\odot$ (km s^{-1})	$\|i_2\|$ (deg)	$\chi_{\odot 2}$ (deg)	f_{R2} (km s^{-1})	$f_{\vartheta 2}$ (km s^{-1})	$\|i_4\|$ (deg)	$\chi_{\odot 4}$ (deg)	f_{R4} (km s^{-1})	$f_{\vartheta 4}$ (km s^{-1})	min (δ^2)
Self-sustained	26.3 ± 1.3	17.5 ± 0.8	9.9 ± 1.9	-8.8 ± 1.0	11.9 ± 1.1	6.1 ± 0.4	$311. \pm 11.$	0.4 ± 3.0	-14.0 ± 3.0	12.0 ± 0.8	$122. \pm 15.$	0.8 ± 3.3	-10.9 ± 2.9	187.
Bar-dominated......	25.7 ± 1.2	9.8 ± 2.3	-6.8 ± 5.0	-13.6 ± 2.4	9.3 ± 1.2	12.6 ± 0.5	$184. \pm 4.$	12.5 ± 3.8	$-19.4 \pm 4.4.$	12.6 ± 1.0	$8. \pm 7.$	6.6 ± 2.4	-10.1 ± 2.1	220.

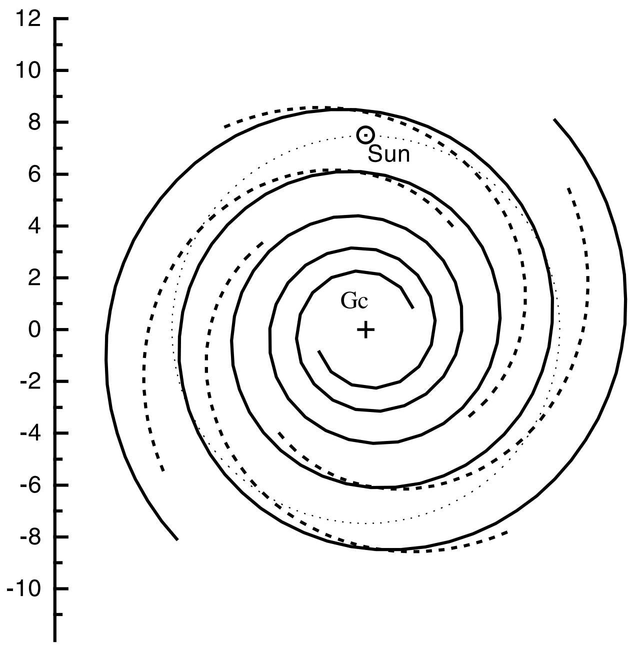

FIG. 2.—Locus of min φ_{S2} and min φ_{S4} on the Galactic plane. The scale is indicated in kpc. As discussed in the text, this does not necessarily correspond to the visible structure.

tic particles moving in a given gravitational field with a potential φ_G defined by equations (1) and (4)–(6). We restrict ourselves to consideration of two-dimensional particle motion in the Galactic plane.

Note that gas-particle simulations in two dimensions are a powerful tool, widely used in the literature (e.g., Combes & Gerin 1985; EG), although the cloud collisions are usually treated in a very simplified manner in these calculations. There are good reasons to believe that diffuse H I clouds exist, as revealed by absorption lines in front of stars (see, e.g., Spitzer 1968, for the parameters of standard clouds). These clouds are expected to collide, mainly in the regions of the disk where the cloud density is high. The physics of cloud collisions is very complicated; in particular, density-dependent cooling rates, chemical transformation of H I into H_2, etc., must be taken into account (see e.g., Marinho & Lépine 2000, for recent simulations). Probably, at the end of the process, new diffuse clouds form from the debris of the collision. However, the only aspect that is of interest here is that the direction of motion and velocity of the resulting new clouds reflect the initial motion of the colliding clouds. About the same effect is obtained in a much simpler way by describing the collision as being "inelastic." Since we do not pose the task of investigating the evolution of the Galactic interstellar medium, only the simplest approach will be exploited here. We do not take into account numerous processes like cloud interactions with expanding envelopes of supernovae, formation of molecular complexes and star birth, mutual cloud gravitation, etc. The only effect which will be considered is that during a collision, the clouds loose energy, but momentum is conserved.

Let us briefly describe the details of the calculations. The computations are performed in a frame of reference corotating with spiral arms. The coefficient of inelasticity (f_r in RH's designation) was chosen to be equal to 0.8. For the mean-free path we adopt the value 300 pc (note that as was shown by RH, the resulting large-scale structure depends very little on the exact value of this quantity).

At the initial moment of time ($t = 0$) the spiral perturbations are assumed to be absent ($\varphi_S = 0$). N particles ($N = 4 \times 10^4$) are uniformly distributed over a disk within $R < 13$ kpc. Each particle is given the local rotation velocity, disturbed by a chaotic velocity with one-dimensional dispersion 8 km s^{-1} (the value intermediate between the ones adopted by RH and Combes & Gérin 1985).

For $t > 0$ the spiral perturbation is "switched on" according to a law

$$\varphi_S = (1 - e^{-0.2\Omega_\odot t})(\varphi_{S2} + \varphi_{S4}) , \tag{18}$$

where φ_{Sm} are taken from equation (5). Our task is to compute the reaction of the system on this perturbation (the N-body problem for particles moving in an external field).

The parameters both for unperturbed and for perturbed potential were taken from Table 1. For $R > 9.4$ kpc the rotation curve was continued by a flat part.

The self-sustained galactic waves are well known to exist between the inner and the outer Lindblad resonances. Since we are not interested in the processes in the central part of the Galaxy, the spiral perturbation was cut off for $R < 2$ kpc. For the spiral gravitational amplitude A_2 we assumed the "standard" value: $2A_2 \cot i_2/\Omega_\odot^2 R_\odot^2 = 0.05$ (LYS).

The result of our simulation of particle-cloud dynamics in the spiral gravitational field for the superposition of 2+4 self-sustained density wave harmonics is shown in Figure 3. In a significant range of Galactocentric distances the pattern looks like a 4-armed one. But we do not face the problem of too short arms, as we would in the case of pure $m = 4$ harmonics (see also AL). Our pattern reflects the complicated picture often observed in external galaxies, e.g., arm bifurcation or their overlapping. Notice a good agreement in major features of our pictures with the pattern for the Galaxy in Figure 3 of Efremov (1998).

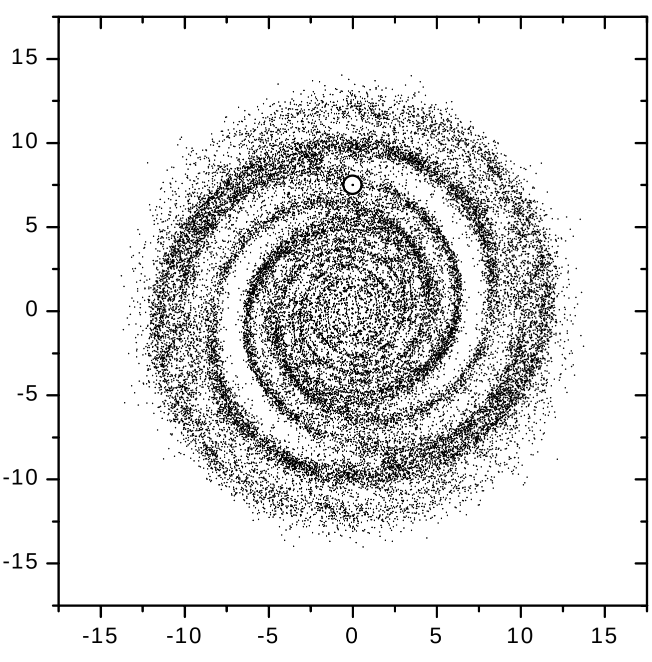

FIG. 3.—Visible structure of the Galaxy derived for the best model (superposition of 2+4 self-sustained wave harmonics) by means of cloud-particle simulation. The scale is indicated in kpc. Note that the model is not valid for radii smaller than about 2.5 kpc.

Although the purpose of the simulation is only to reveal the structure derived by another method (the Cepheid kinematics), our results can be compared with those of EG, since both works use a multipole expansion of the spiral potential, with 2-armed and 4-armed components. EG make use of a SPH code, contrary to our more simplified gas-particle analysis, but this is not the origin of the large differences in the results. EG focus the bar and the central parts of the Galaxy, and adopt a particular model for the mass distribution in that region, with a rotation curve that decreases toward the center, in the inner 1 kpc. Note that this potential is not universally accepted (e.g., Lépine & Leroy 2000). EG favors a model with a pattern speed of 60 km s^{-1} kpc^{-1}, compared to 26 km s^{-1} kpc^{-1} in our case, and a corotation radius of 3.4 kpc, compared to 7.5 kpc in our case. In this work, we present new arguments as well as previous references in favor of the corotation being close to the Sun.

5. GAP IN THE GALACTIC GASEOUS DISK AS AN INDICATOR FOR THE COROTATION CIRCLE

One of the most important conclusions of § 3 is that the Sun lies very close to the corotation radius (see also Marochnik et al. 1972; CM; MZ; AL; etc.). In this section we present a new test which makes it possible to localize directly the position of the corotation circle in a spiral galaxy.

Many years ago Kerr (1969) paid attention to a ringlike region which is markedly deficient in neutral hydrogen, with radius slightly greater than the solar distance from the Galactic center (see also Simonson 1970). This result was later supported in more detail by Burton (1976). He showed that there is a very clear gap in radial distribution of atomic hydrogen in our Galaxy at $R \approx 11$ kpc, whereas in the old scale, used in that paper, $R_\odot = 10$ kpc (see Fig. 6 of Burton 1976). In general, the gap reminds one of the Cassini gap in the Saturnian rings. Such a minimum in the radial H I density profile is observed in external galaxies as well, and demands an explanation. For instance, in a sample of six Sb type field galaxies investigated by Cayatte et al. (1994), two show a clear minimum at a radius about 0.7 times the optical radius (their Fig. 7). This would correspond to about 8.4 kpc in our Galaxy, considering an optical radius of 12 kpc.

It is natural to connect this gap in the radial ISM distribution with the process occurring at corotation: the gas is pumped out from the corotation under the influence of the gravitational field of spiral arms (see also Suchkov 1978; Goldreich & Tremaine 1978; Gor'kavyi & Fridman 1994). The qualitative explanation is as follows. It is well known that when the gas flows through the galactic density waves, a shock arises in the medium (Roberts 1969; RH). Since the Galactic disk rotates differentially, and for $R < R_c$ Ω is greater than Ω_p, the gas in this region overtakes the spiral wave, entering it from the inner side. In the shock the clouds are decelerated, and fall toward the Galactic center. For $R > R_c$ Ω is less than Ω_p, and the process is inverse. Here the wave overtakes the gas and pushes it. So, the clouds pass to an orbit more remote from the Galactic center.

Our simulation of gas-cloud dynamics in the spiral gravitational field directly demonstrates this phenomenon. We show in Figure 4 the radial gas distribution ($\langle n \rangle$ is the particle concentration averaged over a circle) for $t = 0$ and $t = 3.0$ (the time is given in rotation period at the solar distance) for the best parameters of § 3. The gap in the ISM distribution at the corotation radius is well seen. Comparison of our Figure 4 with Figure 6 of Burton (1976) shows a close similarity between them. The H II density profiles also resemble that of the galaxies observed by Cayatte et al. (1994), mentioned above.

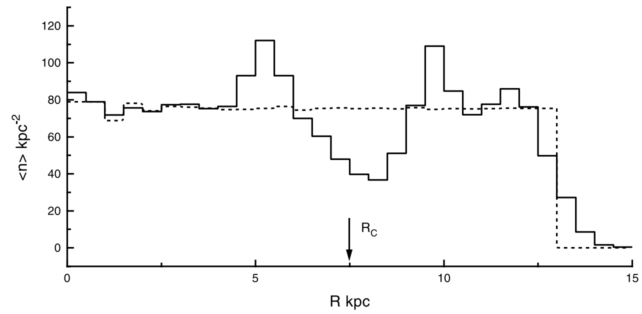

FIG. 4.—Radial distribution of cloud concentration $\langle n \rangle$ (averaged over a circle) for $t = 0$ (*dashed line*) and after the perturbation was switched on, at $t = 3.0$ (in units of Galactic rotation period at solar radius) (*solid line*). The gap in the gas distribution is clearly seen near the corotation radius R_c. The Sun is situated at $R_\odot = 7.5$ kpc.

This result enables us to explain another problem as well. It is well known that the rotation velocity of the disk presents a sharp minimum near the solar-galactocentric distance; the minimum appears independently of the tracer being gaseous (e.g., Honma & Kan-ya 1998) or stellar (Amaral et al. 1996). This phenomenon could be thought to be understood in terms of the velocity perturbation from the galactic density waves, or from the rising effect of a dark matter component at distances larger than the solar radius. Amaral et al. (1996) exclude these hypotheses in their discussion of the nature of this minimum. Now, if there is a ringlike region devoid of gas, in principle the rotation velocity could not be measured in that region using a gas tracer. Similarly, if one selects short-lived stars as tracers, these stars are not expected to form and to exist inside that region, because of the gas deficiency and the very low velocity of the gas with respect to the spiral pattern, which turns the gas compression (the star-formation process) inefficient. It is therefore probable that the gas clouds and the stars that we observe inside the gap are objects with noncircular orbits that invade the gap; they are observed close to their maximum elongation and, therefore, present a lower velocity than the circular one, in the direction of rotation.

So a ringlike gap in the galactic gaseous disk, and possibly also a sharp minimum in the rotation curve, may serve as independent indicators for localization of the corotation circle in a spiral galaxy.

6. NEW SPIRAL STRUCTURE OF THE GALAXY DERIVED FROM H II DATA

Since the discussion in the previous sections proposes a new description of the spiral structure, based on a study of stellar kinematics, it is of great interest to verify whether our results are supported by direct observations of spiral tracers. As a first step, we are only willing to see whether the spiral tracers give some support to a 2+4-armed model. We intend to study not velocity perturbations, as in § 4, but the observed position of the arms. Note that any well-accepted tracer of the spiral structure could be used for such a study. We believe that the Galaxy has a real spiral structure, the same structure being revealed by any type of young object. This view is supported by the fact that different tracers present the same tangential directions (see, e.g., Table 1 of Englmaier & Gerhard 1999). The reason for this is that star formation occurs almost only in spiral arms, and because of their initial velocities, the young objects take a long time before they leave the arms (see the discussion on the formation of the gap in § 5).

The H II regions are the best tracers of the large-scale spiral structure, since they can be observed at large distances, and unlike H I, they are sharply concentrated in the arms (e.g., GG). We performed a new analysis of the sample of H II regions of the Galaxy, without making use of the results of the theoretical models discussed in this paper, except for one hypothesis, namely, that the structure can be represented by a superposition of 2+4-armed patterns. Therefore, the results of this section constitute an independent test of the previous ones.

The procedure adopted is to trace tentative spiral arms in the Galactic plane, and to transform X-Y positions along the arms into the locus of the arms in the l-v diagram, by means of the rotation curve. Note that one position in the X-Y plane gives a unique point in the l-v diagram; there is no problem of distance ambiguity when going in this direction. By varying the parameters of the arms, we looked for the best fit to the l-v diagram. It is well known that the arms that are situated inside the solar circle transform into narrow loops in the l-v diagram, the extremity of a loop corresponding to a tangential direction in the Galactic plane. The spiral pattern is represented by the sum of the $m = 2$ system (two identical long arms with a phase difference of 180°) and of the $m = 4$ system (four identical short arms each separated by 90° in phase) shifted by some phase angle from the first system. The adjusted parameters are the pitch angles, the angle for the phase shift, and the inner and outer radii of each of the two systems. Note that the last four parameters (the radius range) do not affect the quality of the fit, in the usual sense. The only effect is that if we take too large a range, we produce prolongation of arms where they are not needed.

We used the catalog of 726 H II regions of Kuchar & Clark (1997). The l-v diagram with the fitted loops is shown in Figure 5. The rotation curve, that we adopted for the position-velocity transformation, was derived from the interstellar gas data of Clemens (1985), reinterpreted in terms of $R_{\odot} = 7.5$ kpc. We preferred to use a well-accepted rotation curve directly based on observational data, rather than the curve derived in the previous sections, so that the results of this section can be regarded as a totally independent proof that a 2+4-armed structure is a satisfactory one.

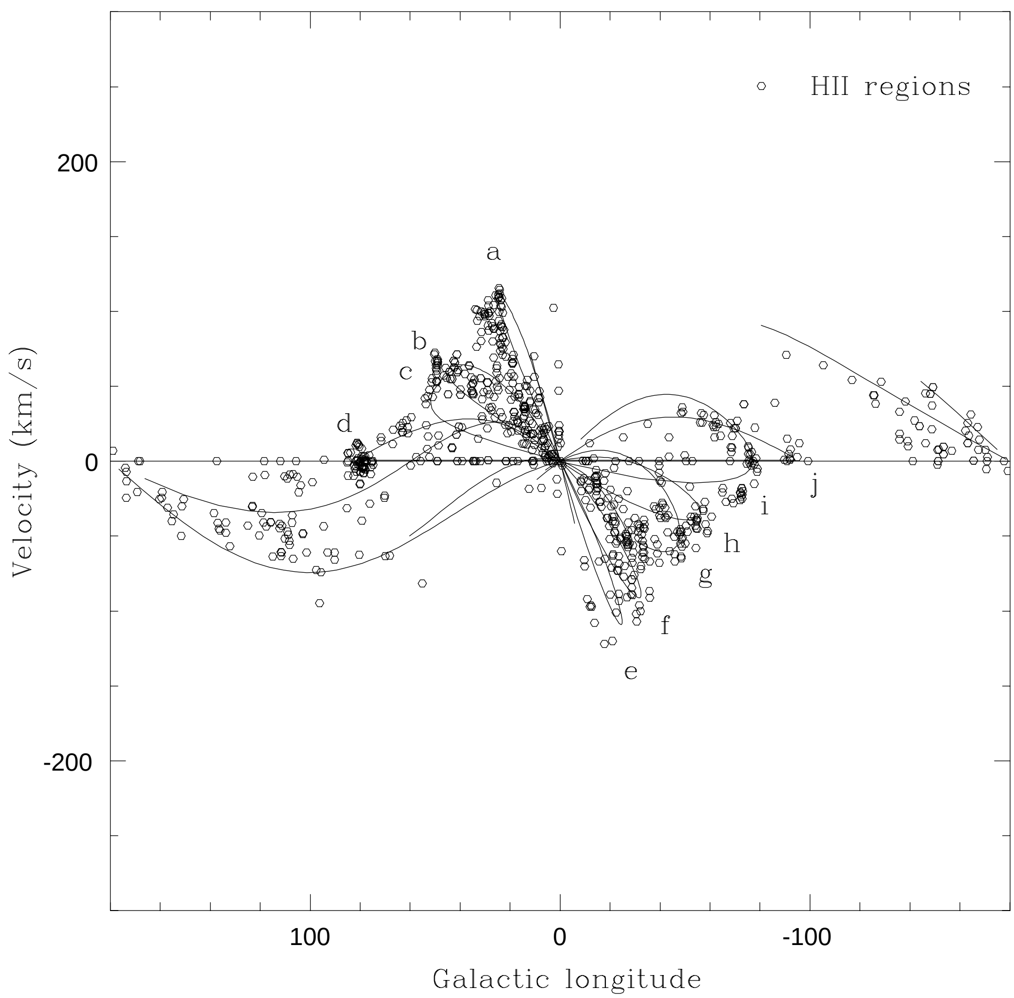

FIG. 5.—Observed l-v diagram for H II regions (from Kuchar & Clark 1997) and the loops that we fitted empirically with a 2+4-armed structure. The letters a, b, c, etc., help to identify the corresponding tangential directions to spiral arms in Fig. 6. Note that d and i are part of the same loop and are connected by a line which is superimposed on the zero-velocity axis.

We must say, however, that the observed curve and the curve derived from the Cepheid kinematics are similar, the only important differences occurring outside the radial range of interest.

The loops are labeled *a* to *j* in the *l*-*v* diagram; the corresponding positions of the tangential points are indicated on the pattern in the Galactic plane in Figure 6.

We next discuss some of the features of the proposed structure. In the region $l = 340°$–$270°$, which is the only region where clear arms were observed by GG, the structure resulting from our study closely resembles that of these authors, presenting about the same tangential directions. Remark that the longitudes of tangential directions are not affected by a change of distance scale (GG used $R_\odot = 10$ kpc). Therefore, in this range of longitude, it is almost impossible to distinguish between the 2+4-armed model that results from our study and the empirical model of GG. We must remember that the arms are not very thin, so that close arms are not resolved. A difference between GG's and our work is that GG did not indicate the existence of a tangential direction at about $l = 338°$ (our inner loop *e*), but obviously there are observed H II regions in that direction, at large negative velocities, that justify our model. In some other directions, the observations favor our model as well. Remark for instance that there are concentrations of H II regions near labels *d* and *j* in Figure 5. These are well explained by a spiral arm that passes very close to the Sun, seen almost at $l \approx +90°$ and then at $l \approx -90°$. Note that the velocities are almost zero in these directions, for distances that are not too large, according to the well-known expression $v \propto \sin 2l$. The longitudes of the tangential directions indicate that this arm has a small pitch angle (about 6°). On the contrary, the wide-loop label *i*, can only be reproduced with a larger pitch angle (12°–14°). This emphasizes the need for arms with different pitch angles.

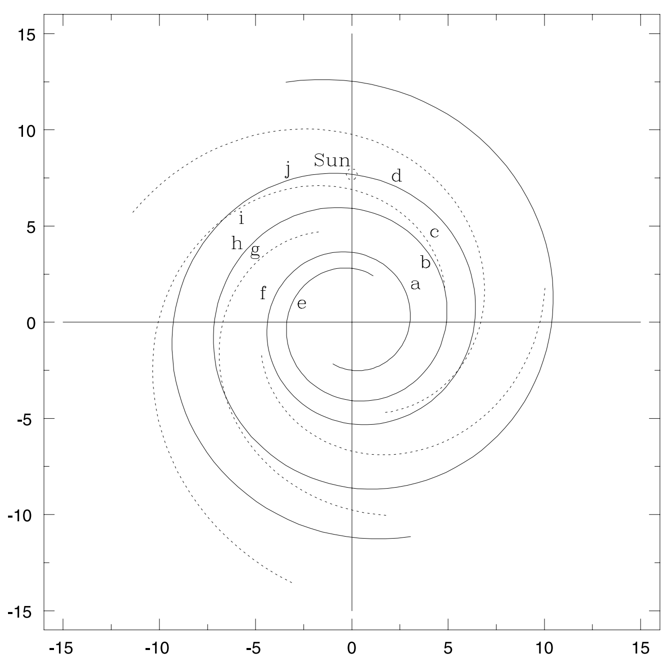

FIG. 6.—Spiral structure of the Galaxy derived from the sample of H II regions. The scale is in kpc. The arms corresponding to the 4-armed component are shown as dotted lines. The spiral arms transform into the loops shown in Fig. 5, using the rotation curve and the geometry to calculate the observed velocity along the arms. Notice the similarity to Fig. 3, although obtained in a completely independent way.

The best fit of the *l*-*v* diagram of the observed H II regions that we obtained with the simple 2+4-armed model is not perfect. For instance, loop *a* would give a better fit of the H II regions if shifted toward larger longitudes, and loops *i* to *e* would produce a better fit if displaced toward smaller velocities. This probably occurs because the real Galaxy cannot be represented by perfect logarithmic spirals, and we did not take into account the existing velocity perturbations with respect to the rotation curve. Despite these small shifts, the fit is qualitatively correct and reproduces the main features of the diagram and, in particular, the main known tangential directions (see, e.g., Table 1 of Englmaier & Gerhard 1999). It is remarkable that this result was obtained with pitch angles 6°.8 for the 2-armed component and 13°.5 for the 4-armed component, similar to those obtained in § 4. We emphasize that the results of this section are totally independent of those based on stellar kinematics.

Turning to other tracers, it must be said that the H I and CO *l*-*v* diagrams do not seem to be as convenient as H II regions to trace the spiral structure. This occurs because the H II regions are discrete sources always related to star formation, while H I and possibly CO can be found in the inter arm regions as well. Furthermore, the 21 cm line and the ^{12}CO lines are often optically thick, so that they do not preserve very well the information on the amount of matter as a function of the position. Finally, the *l*-*v* diagrams are often presented only for $b = 0°$, so that spiral arms that are slightly displaced from the Galactic plane are partially lost. Despite these difficulties, some comparisons can be made. For instance, Feitzinger & Spicker (1985, hereafter FS) present a view of the Galactic plane with the position of H I centroids, that take into account the displacements in the *z*-direction. If we move out from the Galactic center toward the left, in Figure 8 of FS, we cross a total of four well-behaved, almost concentric arms, the last one situated at a distance slightly larger than $R_\odot$ from the Galactic center. This is very similar to what we propose in our Figure 6, remembering that arms that are very close together are not resolved. These structures are qualitatively different from those produced in the model of EG.

We can also recognize the features delineated by H II regions as described above, in the CO *l*-*v* diagrams of Dame et al. (1987) (see also the *l*-*v* diagram from unpublished data by Dame et al. 1987, reproduced by EG). If we exclude the central regions (within $-10° < l < 10°$) that we are not studying here, we recognize loop *a* at about $l = 30°$, $v = 100$ km s^{-1}, extending to loop *e* at about $l = -20°$, $v = -100$ km s^{-1}. In the CO *l*-*v* diagram the connection from *a* to *e* or *f* crosses the zero longitude axis at negative velocities (about -50 km s^{-1}). This is well explained for orbits close to the inner Lindblad resonance (see, e.g., Fig. 10 of AL); remember that in our Figure 5 we have not considered any velocity deviation from pure circular motion. Loop *i*, with positive velocities near $l = -60°$, can also be seen in the CO *l*-*V* diagram reproduced by EG.

According to our model, an arm passes very close to the Sun, slightly inside the solar Galactic radius. We identify this with the arm clearly delineated by molecular clouds, from the Cygnus Rift to the Vela Sheet, passing about 150 pc from the Sun (see Fig. 7 of Dame et al. 1987). If we go farther from the Sun, toward the Galactic center, according to our picture, we should meet another arm at about 1 kpc,

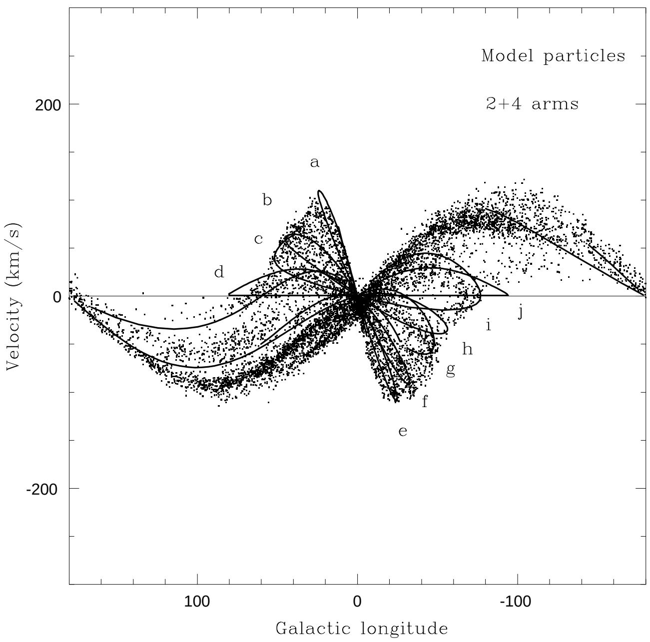

FIG. 7.—Theoretical *l*-*v* diagram computed by means of particle-cloud simulation for the best model: superposition of 2 + 4 self-sustained wave harmonics. The lines represent the fit to observed H II regions, from Fig. 5. These lines are shown as guide lines that are useful for comparison of different models presented in the next figures, and of the models with the H II regions distribution.

and still another one at an additional distance of 1 kpc. Although it is difficult to recognize an arm seen face-on, and kinematical distances cannot be used in directions close to $l = 0°$, the studies of interstellar extinction as a function of distance from the Sun by Neckel & Klare (1980) show a clear increase at 1 kpc (see, e.g., their plots for directions $l = 336°$, $338°$, $340°$, $353°$, etc.). The second step at 2 kpc from the Sun is obviously more difficult to map though interstellar extinction, but can be recognized in the extinction plots of Neckel & Klare toward $l = 349°$, $360°$, $11°$, and $13°$.

In summary, in this section we have shown that the main aspects of the galactic structure traced by H II regions, and also by other tracers and by the known tangential directions, are well described in terms of an empirical 2 + 4-armed model.

7. COMPARISONS WITH THEORETICAL *l*-*v* DIAGRAMS

In § 4 we were working with gas particles that have no special reason to be considered as young objects. Since the galactic gas transforms from H I to H_2 and vice versa, and our particle model does not consider chemical reactions, we should not expect much similarity between our theoretical *l*-*v* diagrams and those of CO or H I surveys. However, we must remember that a region in the Galactic plane where the gas particles appear densely packed is a region where cloud collisions have a high probability to occur, and therefore it is a region of star formation. If detailed physics were taken into account, we would find young tracers at these places. So it is fair to compare structures formed by high densities of gas particles with structures delineated by young objects.

A second consideration is that such comparisons as a longitude-velocity diagram obtained by a gas particle simulation with that of an observed spiral tracer, or of the positions of spiral tracers in the Galactic plane versus positions from a model, are almost always qualitative. But still, qualitative comparisons are of great value. By comparing simulations performed by different authors, we immediately recognize the main differences. Many models could be easily rejected, on the basis of a simple visual inspection of their predictions, compared to observed tracers.

Let us now discuss the theoretical *l*-*v* diagrams that were computed by means of our particle simulations in § 4, shown in Figures 7–9. Since it is difficult to superimpose the particle distributions from different simulations for comparison, we plotted on these figures the same loops derived for H II regions in the previous section, as eye guides. For a comparison between the H II regions and the theoretical *l*-*v* diagrams, we can use these lines as well, but we also present a direct superposition of the 2 + 4-armed model *l*-*v* diagram with the H II regions in Figure 10. In this case, we reduced the number of particles shown, to avoid crowding.

Figures 7 and 8 are very similar between themselves, and similar to the observed diagram for H II regions, in many aspects. In particular, the observed loops labeled *a*, *b*, *d*, *e*, *f*, *g*, *i*, *j* can be seen to correspond to enhanced particle densities. A difference that appears between the theoretical *l*-*v* diagrams and the observed ones for H II regions is a strong concentration of gas particles along the line from $l \approx 80°$, $v \approx -100$ km s^{-1} to $l \approx -80°$, $v \approx +100$ km s^{-1}, where no H II regions are observed. This difference can be easily explained, and does not mean that the theoretical model is incorrect. In our particle simulations, we distributed the particles over a large radius range, because the particles are supposed to represent the gas in all its forms including H I clouds, and H I is known to exist at large radii. The strong concentration of gas particles corresponds to particles situated at large distances from the center (the

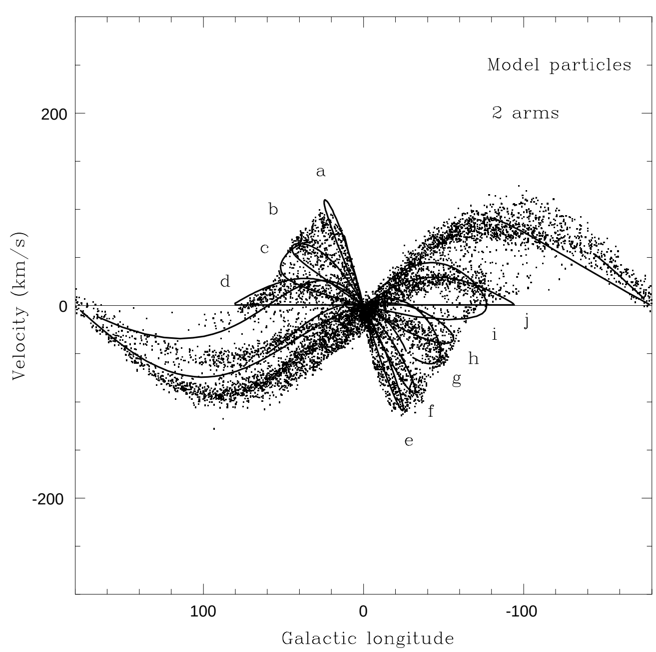

FIG. 8.—Same as Fig. 7, but for the model of pure $m = 2$ wave harmonic (the parameters for the particle simulation made in the present work were taken from Mishurov et al. 1997). The lines represent the fit to observed H II regions, from Fig. 5, for comparison, and not a fit to the $m = 2$ model.

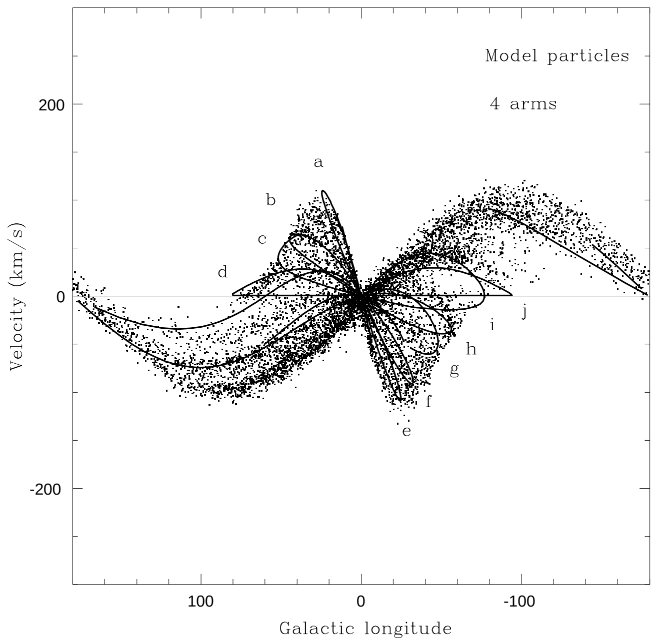

FIG. 9.—Same as Fig. 8, but for the model of pure $m = 4$ wave harmonic (the parameters were taken from MZ). The lines represent the fit to observed H II regions, from Fig. 5, for comparison, and not a fit to the $m = 4$ model.

kinematical distance is easily derived), whereas it is known that there is a lack of H II regions at large radii.

It is not surprising that the *l-v* diagrams in Figures 7 and 8 are so similar, since the two models contain similar 2-armed components, and this component is prominent over a wider galactocentric region than the 4-armed component of the 2+4-armed model. However, we can point out some subtle differences. For instance, the arm that passes very close to the Sun, as discussed above (loops *d* and *j*), appears more clearly in the 2-armed model (Fig. 8). We must emphasize that the loops presented in Figures 7–9 are eye guides; they are not perfect fits to the H II region. In particular, in the observed H II regions diagram (Fig. 5) we can see many objects between the two lines shown in the longitude range $l = 160°$–$80°$. The same happens in Figures 7 and 8, which show the results of the simulations. Similarly, we can see many H II regions between loops *f* and *g*, in Figure 5, that are not well fitted by the loops, and we can also see many objects in this region in Figure 7, the theoretical self-sustained model. The gas particles coincide better with the H II regions around position *e* (Fig. 10) than the loop shown in Figure 5. In other words, the theoretical 2+4-armed model is closer to observations than the "empirical" fit represented by the lines, in a number of details. Furthermore, around longitude 240° (or $-120°$), the theoretical *l-v* diagram of the 2+4-armed model shows a

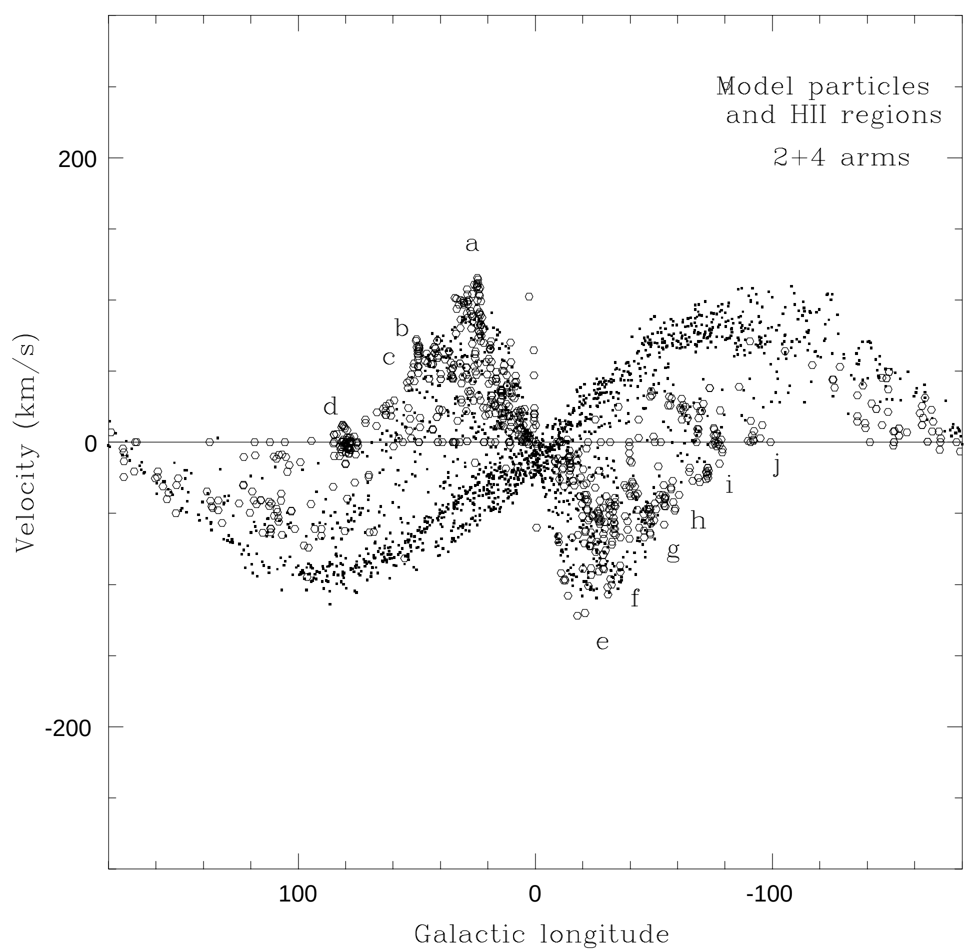

FIG. 10.—Same theoretical *l-v* diagram of Fig. 7, with the H II regions superimposed (*open circles*) for direct comparison. In order to avoid crowding, only a fraction of the cloud particles are represented (*dots*), randomly selected from the original sample. The concentration of cloud particles without corresponding H II regions from about 80°, -100 km s^{-1} to $-80°$, $+100$ km s^{-1} is explained in the text.

number of particles with velocities of the order of 30 km s^{-1}. These objects seem to delineate a spiral arm that is not seen in the H II regions diagram. However, an arm indeed exists at this position, as can be seen in the longitude-velocity diagram of *IRAS* sources given by Wouterlout et al. (1990). This arm is deficient in H II regions, probably because of the proximity of corotation.

The 4-armed model (Fig. 9) shows relatively larger differences with observations than the other ones. For instance, the particles do not show the loops *i*, and the concentration of particles near position *b* is less pronounced.

In summary, the pure 2-armed model and the self-sustained 2 + 4-armed model produce theoretical *l-v* diagrams that are similar to each other and similar to that of observed H II regions. The only striking difference between the theoretical and observed diagrams is an expected one, due to the fact that we are comparing objects that behave differently in a region of the disk (H II regions do not form at large radii) If we look into subtle details, the 2 + 4-armed self-sustained model is favored. However, the choice in favor of the 2 + 4-armed model, compared to the pure 2-armed one, is dictated much more strongly by the study of Cepheid kinematics, and by the empirical fit to the H II regions and tangential directions, than by a comparison between theoretical and observed *l-v* diagrams.

8. CONCLUSION

In the present research a new approach to the problem of the galactic spiral structure was proposed in order to construct a more realistic picture like that often seen in external galaxies: coexistence of different spiral systems in a galaxy, arm bifurcation and their overlapping. Our theoretical considerations show that superposition of self-sustained spiral wave harmonics could explain some of the above features, since different azimuthal wave harmonics have different pitch angles.

In the framework of the simplest model of superposition of 2 + 4-armed spiral wave harmonics, we analyzed the best up-to-date data on stellar kinematics, which is the sample of Cepheid stars, with proper motions determined by *Hipparcos*. We examined two models, the self-sustained and the bar-dominated waves. This study complements the previous studies of pure 2-armed and pure 4-armed presented by MZ and Mishurov et al. (1997). Of the four models now available, clearly the one that gives the best fit to the Cepheid kinematics is the self-sustained model, which is a superposition of two arms with pitch angle about 6° and four arms with pitch angle about 12°. We performed *N*-particle simulations to make visible the structure of the potential derived from the Cepheid kinematics for the four models, and to construct the corresponding *l-v* diagrams.

As an independent test of a 2 + 4-armed model, we performed a new analysis of the *l-v* diagram of the Galactic H II regions, which are the best tracers of the large-scale spiral structure. We fitted the observed *l-v* diagram empirically with the loci of spiral arms, using a 2 + 4-armed model. Coincidentally, the best empirical fit was again found using pitch angles about 6°.5 and 13°.5. We also compared the theoretical *l-v* diagrams from the particle simulations with the loci of arms derived from H II regions. Although the differences between *l-v* diagrams of the theoretical models (pure 2-armed, pure 4-armed, and two different 2 + 4-armed models) are not striking, the 2-armed model and the self-sustained 2 + 4-armed models are the ones that produce theoretical *l-v* diagrams most similar to that of the H II regions.

Of all the arguments that we examined, the significantly better fit of the kinematics (the statistical analysis) of Cepheids with the 2 + 4-armed, self-sustained model, is the most convincing one, but clearly the analysis of the sample of H II regions gives support to our interpretation. Although the Galaxy probably shows some deviations from any simplified model, the 2 + 4-armed model with different pitch angles is the one that constitutes the best approach, being consistent with observations and with spiral wave theory. This is the simplest model that can be proposed, apart from pure harmonic modes. Our model does not exclude the existence of higher modes, that are allowed to exist near corotation, but these modes are probably less significant than the first harmonics. It is interesting to remark that our model is able to reconcile the first model of LYS, which has 2 arms with pitch angle 6° similar to our 2-armed harmonic, with the need to satisfy Kennicutt's (1982) correlation between pitch angle and maximum rotation velocity, which predicts a pitch angle of about 14° for our Galaxy, not very different from that of our 4-armed harmonic.

As a by-product of the study, our particle simulation shows that a deficiency of interstellar gas must occur near corotation. This explains the gap in the H I distribution observed by Kerr (1969) and by Burton (1976). This effect is also possibly related to the sharp minimum in the rotation curve near the solar radius discussed by Amaral et al. (1996), also seen in the curve by Honma & Kan-ya (1998). In external galaxies, a ringlike gap in the H I distribution such as that oberved in two field Sb galaxies by Cayatte et al. (1994) may directly show the localization of the corotation circle.

Our investigation of Cepheid kinematics points out that the Sun lies very close to the corotation circle. This conclusion is supported by the solar closeness to the ringlike region of H I deficiency in the Galaxy, by the position of the inner and outer Lindblad resonances and by direct measurement of the pattern speed using open clusters (AL).

This work was partially supported by the Russian Federal Program "Integration" (grant A-007/2000).

REFERENCES

Amaral, L. H., & Lépine, J. R. D. 1997, MNRAS, 286, 885 (AL)
Amaral, L. H., Ortiz, R., Lépine, J. R. D., & Maciel, W. J. 1996, MNRAS, 281, 339
Bash, F. N. 1981, ApJ, 250, 551
Berdnikov, L. N. 1987, Perem. Zvezdy, 22, 505
Berdnikov, L. N., Efremov Yu. N., Vozyakova, O. V., & Dambis, A. K. 1996, Astron. Lett., 22, 936
Burton, W. B. 1976, ARA&A, 14, 275
Caldwell, J. A. R., & Coulson, I. M. 1987, AJ, 93, 1090
Cayatte, V., Kotanyi, C., Balkowski, C., & van Gorkom, J. H. 1994, AJ, 107, 1003
Clemens, D. P. 1985, ApJ, 295, 422
Combes, F., & Gerin, M. 1985, A&A, 150, 327
Crézé, M., & Mennessier, M. O. 1973, A&A, 27, 281
Dambis, A. K., Mel'nick, A. M., & Rastroguev, A. S. 1995, Astron. Lett., 21, 291
Dame, T., et al. 1987, ApJ, 322, 706
Draper, N. R., & Smith, H. 1981, Applied Regression Analysis (New York: Wiley)
Efremov, Yu. N. 1998, A&A Trans. (New York: Gordon & Breach), 15, 3
Englmaier, P., & Gerhard, O. 1999, MNRAS, 304, 512 (EG)
ESA. 1997, The *Hipparcos* Catalogue (ESA SP-1200; Noordwijk: ESA)
Feast, M., & Whitelock, P. 1997, MNRAS, 291, 683
Feitzinger, J. V., & Spicker, J. 1985, MNRAS, 214, 539 (FS)

Georgelin, Y. M., & Georgelin, Y. P. 1976, A&A, 49, 57 (GG)
Goldreich, P., & Tremaine, S. 1978, Icarus, 34, 227
Gor'kavyi, N. N., & Fridman, A. M. 1994, Physics of Planetary Rings: Celestial Mechanics of Continiuous Medium (Moscow: Nauka)
Gorynya, N. A., Samus, N. N., Rastorguev, A. S., & Sachkov, M. E. 1996, Astron. Lett., 22, 198
Honma, M., & Kan-ya, Y. 1998, ApJ, 503, L139
Kennicutt, R. C. 1982, AJ, 87, 286
Kerr, F. J. 1969, ARA&A, 7, 39
Kuchar, T. A., & Clark, F. O. 1997, ApJ, 488, 224
Lépine, J. R. D., & Leroy, P. 2000, MNRAS, 313, 263
Lewis, J. R. 1990, MNRAS, 244, 247
Lin, C. C., Yuan, C., & Shu, F. H. 1969, ApJ, 155, 721
Marinho, E. P., & Lépine, J. R. D. 2000, A&AS, 142, 165
Mark, J. W.-K. 1976, ApJ, 203, 81
Marochnik, L. S., Mishurov, Yu. N., & Suchkov, A. A. 1972, Ap&SS, 19, 285
Mishurov, Yu. N., & Zenina, I. A. 1999, A&A, 341, 81 (MZ)
Mishurov, Yu. N., Zenina, I. A., Dambis, A. K., Mel'nik, A. M., & Rastorguev, A. S. 1997, A&A, 323, 775
Neckel, Th., & Klare, G. 1980, A&AS, 42, 251
Olling, R. P., & Merrefield, M. R. 1998, MNRAS, 297, 943
Ortiz, R., & Lépine, J. R. D. 1993, A&A, 279, 90
Pont, F., Mayor, M., & Burki, G. 1994, A&A, 285, 415
Puerari, I., & Dottori, H. A. 1992, A&AS, 93, 469
Reid, M. J. 1993, ARA&A, 31, 345
Roberts, W. W. 1969, ApJ, 158, 123
Roberts, W. W., & Hausman, M. A. 1984, ApJ, 277, 744 (RH)
Shu, F. H. 1970, ApJ, 160, 99
Simonson, S. C. 1970, A&A, 9, 163
Spitzer, L., Jr. 1968, Diffuse Matter in Space (New York: Wiley)
Suchkov, A. A. 1978, AZh, 55, 972
Vallée, J. P. 1995, ApJ, 454, 119
Wouterlout, J. G. A., Brand, J., Burton, W. B., & Kwee, K. K. 1990, A&A, 230, 21